Journal of Controlled Release 161 (2012) 735–745

Contents lists available at SciVerse ScienceDirect

Journal of Controlled Release

journal homepage: www.elsevier.com/locate/jconrel

NANOMEDICINE

Enhanced skin permeation using polyarginine modified nanostructured lipid carriers

Punit P. Shah [1], Pinaki R. Desai [1], Debra Channer, Mandip Singh *

College of Pharmacy and Pharmaceutical Sciences, Florida A&M University, Tallahassee, FL 32307, USA

ARTICLE INFO

Article history:
Received 19 March 2012
Accepted 5 May 2012
Available online 14 May 2012

Keywords:
Skin delivery
Nanostructured lipid carriers (NLC)
Cell penetrating peptide (CPP)
Allergic contact dermatitis (ACD)
Polyarginine peptide

ABSTRACT

The objective of the present study was to investigate the effect of polyarginine chain length on topical delivery of surface modified NLCs. Design of experiments (DOE) was used to optimize number of arginines required to deliver active drug into deeper skin layers. The NLCs were prepared by hot-melt technique and the surface of NLCs was modified with six-histidine tagged cell penetrating peptides (CPPs) or YKA. *In vivo* confocal microscopy and Raman confocal spectroscopy studies were performed using fluorescent dye encapsulated NLCs and NLC-CPPs. Spantide II (SP) and ketoprofen (KP) were used as model drugs for combined delivery. *In vitro* skin permeation and drug release studies were performed using Franz diffusion cells. Inflammatory response corresponding to higher skin permeation was investigated in allergic contact dermatitis (ACD) mouse model. NLCs had a particle size of 140 ± 20 nm with higher encapsulation efficiencies. The negative charge of NLC was reduced from -17.54 to -8.47 mV after surface modification with CPPs. *In vivo* confocal microscopy and Raman confocal spectroscopy studies suggested that a peptide containing 11 arginines (R11) had significant permeation enhancing ability than other polyarginines and TAT peptides. The amount of SP and KP retained in dermis after topical application of NLC-R11 was significantly higher than solution and NLC after 24 h of skin permeation. SP was not found in receiver compartment. However, KP was found in receiver compartment and the amount of KP present in receiver compartment was increased approximately 7.9 and 2.6 times compared to the control solution and NLCs, respectively. In an ACD mouse model, SP + KP-NLC-R11 showed significant reduction ($p<0.05$) in ear thickness compared to SP + KP solution and SP + KP-NLC. Our results strongly suggest that the surface modification of NLC with R11 improved transport of SP and KP across the deeper skin layers and thus results in reduction of inflammation associated with ACD.

1. Introduction

Psoriasis, atopic dermatitis and allergic contact dermatitis are skin disorders that are characterized by chronic inflammation with a significant neurogenic component. Currently, these disorders are principally treated with topical corticosteroids that target a variety of pathways of the inflammatory cascade [1]. However, the corticosteroid therapy is associated with local side effects such as skin atrophy, telangiectasia, acne and secondary infections which may results in contact dermatitis and perioral dermatitis. To overcome unwanted side effects associated with monotherapy, a combination approach is widely used since two disease modifying drugs when used together can act through different pathways and offer possibility for synergistic or additive effects. Spantide II (SP) [2–4] and ketoprofen (KP) [5,6] are well studied for reducing the swelling and inflammation associated with skin disorders. Therefore use of two anti-inflammatory drugs, SP and KP, can modify the inflammation conditions favorably when delivered simultaneously. SP is a peptide that specifically binds to neurokinin-1 receptor (NKR-1) and blocks pro-inflammatory activity associated with Substance P [7]. On the other hand, KP is a potent non-steroidal anti-inflammatory drug (NSAID) which inhibits arachidonic acid metabolism by potent inhibitory actions on cyclooxygenase and lipooxygenase.

In the dermatological treatment, improving clinical efficacy requires high drug levels at specific site of the skin with less systemic absorption. Stratum corneum (SC) is the biggest barrier for skin delivery which reduces the absorption of active drugs in the skin layers [8]. Several approaches have been proposed and are being used to enhance the skin permeation of drugs using either chemical [9,10] and physical enhancement techniques like ultrasound [11], radiofrequency [12], iontophoresis [13,14], magnetophoresis [15], electroporation [16], microneedles [17] but they have their respective limitations in terms of toxicity and therapeutic feasibility. One of the most pursued methods to increase the drug transport across the skin is the use of nanocarriers [18]. The potential of nanosized carriers (liposomes, polymeric and lipid nanoparticles) for topical delivery has been addressed in several studies [19]. Delivery systems such as polymeric nanoparticles or liposomes have limitations in their

* Corresponding author at: College of Pharmacy and Pharmaceutical Sciences, Florida A&M University, Tallahassee, FL 32307, USA. Tel.: +1 850 561 2790; fax: +1 850 599 3347.
E-mail address: mandip.sachdeva@gmail.com (M. Singh).
[1] Contributed equally.

0168-3659/$ – see front matter © 2012 Elsevier B.V. All rights reserved.
doi:10.1016/j.jconrel.2012.05.011

a) industrial applications like physical stability problems with liposomes b) lack of a regulatory acceptance of many polymers and c) high costs for effective large scale production [20]. To overcome these problems, nano lipid carriers (NLCs) have been developed using the blend of both solid lipids and liquid lipids (oils) [21]. NLCs have higher loading capacity and lower drug leaching on storage compared to other lipid nanocarriers. Also, NLCs have demonstrated potential for topical route of application. NLCs are known to improve stability and controlled release of the incorporated drugs [22,23]. In addition, NLCs are well tolerated by skin and easy to scale up [20].

In our efforts to enhance the delivery of lipid nanocarriers into deep epidermis, we have already shown that a well known cell penetrating peptide (CPP), transactivating transcriptional activator (TAT), when linked to NLCs has the potential to carry their payloads across the skin layers [24]. In recent years, CPPs have opened new avenues in the field of drug delivery to deliver various molecules like peptides, proteins, nucleic acids, antibodies and imaging agents across the cellular membranes [25,26]. Several CPPs like polyarginine-7 (R7), polyarginine-9 (R9; NONA), transporter-9, polylysine-9 (K9), penetratin (PEN), and RALA have been studied to enhance the skin delivery of active drugs [19,27,28]. Further the effect of arginine chain length of polyarginines (Rn; $n=4$ to 16) has been widely investigated for improving the permeation enhancing ability and cellular localization of active drugs in cancer cells [29,30]. However, there are no reports available on the use of a polyarginine peptide containing more than 9 arginines to improve skin permeation of active drugs. Therefore a systematic study to investigate the effect of polyarginine chain length containing more than 9 arginines on the skin delivery of cargo molecule needs to be investigated.

The US Food and Drug Administration's Quality by Design (QbD) initiative encourages the use of statistical tools for improving the development of the pharmaceutical formulations with high quality [31]. Design of experiment (DOE), a powerful statistical tool, has been established as a convenient method for developing optimum products precisely and is known to minimize the number of experiments with efficient screening of the process parameters. Further it assures the quality of process or product in terms of mathematical relationships [32]. The results of statistically planned experiments find better acceptance than those of traditional single variable experiments. Therefore, a mixture design was used to optimize number of arginines containing peptide required to deliver a drug into deeper skin layers wherein number of arginines containing peptides and different skin depths were selected as independent variables and percent fluorescence intensity, calculated from confocal images along with Raman intensity were selected as dependent variables. Based on desirability function, the optimum number of arginines containing peptide was selected and used for surface modification of NLCs comprising SP and KP. These surface modified NLCs were then assessed for *in vitro* skin permeation and *in vivo* treatment of inflammatory skin disorder like allergic contact dermatitis (ACD) in mice model.

2. Materials and methods

Miglyol 812 was kindly gifted by Sasol Germany GmbH (Witten, Germany). Precirol, Monosterol and Compritol 888 ATO were gifted by Gattefosse (Saint Priest, France). 1,2-Dioleoylsn-glycero-3-[(N-(5-amino-1-carboxypentyl) imidodiacetic acid) succinyl nickel salt] (DOGS-NTA-Ni), L-phosphatidylinositol (liver bovine sodium salt) (PI), L-phosphatidyl choline (egg-hydrogenated) (PC) were purchased from Avanti Polar lipids (AL, USA). Polyoxyethylene-20 oleyl ether (Volpo-20) was a kind gift from Croda Inc (NJ, USA). The six histidine tagged polyarginine peptides (R8: RRRRRRRR-6 histidine tag), (R11: RRRRRRRRRRR-6 histidine tag), (R15: RRRRRRRRRRRRRRR-6 histidine tag); TAT (YGRKKRRQRRR-6 histidine tag) cell penetrating peptide and YKA peptide (YKALRISRKLAK-6 histidine tag) peptide as a control were custom synthesized by CHI Scientific, Inc (MA, USA). Vivaspin centrifuge filters (Molecular weight Cut-off: 10,000 Da) were procured from Sartorius Ltd, (Stonehouse, UK). Tetrahydrofuran, tween 80, phosphate buffered saline sachets (PBS, pH 7.4), trifluoroacetic acid (TFA), 2,4-dinitrofluorobenzene (DNFB) and dialysis membrane (flat width of 23 mm) were purchased from Sigma-Aldrich Co (MO, USA). HPLC grade of acetonitrile, water and ethanol were purchased from Sigma-Aldrich Co (MO, USA). Ketoprofen was purchased from Spectrum chemical mfg corp. (CA, USA). Spantide II (SP) was purchased from American peptide company Inc, (CA, USA). Topgraf® (tacrolimus ointment 0.1%) was purchased from GlaxoSmithKline Pharmaceuticals Limited (Thane, India). Poloxamer 188 (Lutrol F68) was kindly gifted by BASF Corporation (NJ, USA).

2.1. Animals

Hairless rats (CD®(SD) HrBi, Male) and C57BL/6 mice (6 weeks old, male) (Charles River Laboratories, Wilmington, MA) were grouped and housed ($n=6$ per cage) in cages with bedding. The animals were kept under controlled conditions of 12:12 h light:dark cycle, 22 ± 2 °C and 50 ± 15% RH. The mice were fed (Harlan Teklad) and water ad libitum. The animals were housed at Florida A&M University in accordance with the standards of the Guide for the Care and Use of Laboratory Animals and the Association for Assessment and Accreditation of Laboratory Animal Care (AAALAC). The animals were acclimatized to laboratory conditions for 1 week prior to experiments. The protocol of animal study was approved by the Institutional Animal Care and Use Committee (IACUC), Florida A&M University, FL.

2.2. Preparation of nanoparticles

NLCs were prepared by modified hot melt homogenization technique [24]. Briefly, PC (0.2% w/w) was dispersed in (0.04% w/w) ethanol. To this miglyol (3% w/w) and DOGS-NTA-Ni (0.02% w/w) were added. Ethanol was evaporated by applying mild heating. To this, compritol (7% w/w) or a mixture of precirol (4% w/w) and monosterol (3% w/w) were added with constant heating in water bath, kept at 50–60 °C to melt the solid lipids. This represented a lipid phase. Water phase was prepared separately by dissolving Lutrol® F68 (poloxamer 188) (1% w/w), followed by dispersing span 80 (0.5% w/w) in water. This water phase was also brought to the same temperature as that of lipid phase. Further the water phase was added to lipid phase under high speed mixing (20,000 rpm for 13 min).

DiO- or DID-NLC were prepared using compritol as a core lipid by dissolving dye into the chloroform. To prepare SP-NLC, SP (0.025% w/w) and 40 μl of 25 mg/ml solution of PI were dissolved in 0.04% w/w ethanol and then mixed with lipid phase. Similarly to prepare KP-NLC, KP (0.05% w/w) was dissolved in ethanol and mixed with lipid phase. To prepare SP + KP-NLC, SP and KP were dissolved in 0.04% w/w ethanol and mixed with lipid phase.

For surface modification, 200 μl of prepared NLCs were mixed with 50 μl of 5 mg/ml 6 his-tagged CPPs solution, prepared in water and was incubated for 2 h at room temperature with constant stirring. Freshly prepared NLCs were used for all experiments and surface modification was performed 2 hr before starting the experiment. For all the experiments NLCs or NLC-CPP (nanoparticle dispersion) prepared in water were used without any change in the composition.

KP solution (KP-Solution; 0.05% w/w), SP solution (SP-Solution; 0.025% w/w) and a combination of SP + KP solution (SP + KP-Solution) were prepared by dissolving drugs in 1% w/w ethanol and then adjusting volume with PEG-400.

2.3. Characterization of nanoparticles

The particle size and zeta potential of NLC or NLC-CPP were measured in distilled water using Nicomp 380 ZLS (Particle Sizing Systems,

Port Richey, FL). The Nicomp 380 ZLS analyzer uses dynamic light scattering to obtain the essential features of the particle size distribution. Zeta potential demonstrates the stability of nanoparticle dispersion. In order to verify the total amount of drug present in the system, 0.1 ml of SP-NLC or KP-NLC were dissolved in 0.9 ml of tetrahydrofuran and subsequent dilutions were made with acetonitrile. The samples were then centrifuged at 13,000 rpm for 15 min and 100 μl of supernatant was injected into Waters high-performance liquid chromatography (HPLC). Entrapment efficiency was determined as reported earlier using vivaspin columns, molecular weight cut-off (MWCO) 10,000 Da [24]. The NLC or NLC-CPP (0.5 ml) were placed in the donor compartment of the vivaspin centrifuge filter membrane and centrifuged at 4,500 rpm for 15 min. The amount of SP and KP present in the receiver compartment was estimated using HPLC.

2.4. Response surface methodology (RSM)

Response surface designs describe accurately how responses behave at all values of the studied variables in the experimental region using quadratic polynomial equation. The aim of RSM is to determine the conditions that provide process and product improvement [32]. The objective of the present study was to select the peptide having optimum number of arginine which could transport significant amount of encapsulated drug from the NLCs into the deeper skin layers. R15, R11 and R8 have 15, 11 and 8 arginines, respectively. TAT has 6 and YKA has 2 arginines. However, unmodified NLCs were having no arginines. Therefore, R15, R11, R8, TAT, YKA and unmodified NLCs were represented as 15, 11, 8, 6, 2 and 0 arginines containing peptides, respectively. The lateral skin sections were collected using cryotome from 0 to 20, 21 to 40, 41 to 80, 81 to 120, 121 to 160 and 161 to 200 μm after 24 h of skin permeation with the fluorescent dye containing NLCs or NLC-CPP. The experimental runs were repeated 6 times using different NLCs or NLC-CPP formulations. The percent fluorescence intensity and Raman intensity at different skin depths were used as dependent variables. The coded and actual values of independent variables are reported in Table 1.

The experimental matrixes at 6 levels consisted of 36 runs for dependent variables, as shown in Table 2. All experimental results were computed by statistical software, DOE v6.0.5 (Stat-Ease, Inc., Minneapolis, MN). A classical second-degree model was postulated for each experimental response Yi, as follows:

$$\mathrm{Yi} = b_0 + b_1A + b_2B + b_{11}A^2 + b_{22}B^2 + b_{12}AB + \mathrm{Ei} \quad (1)$$

where b_0 is the arithmetic mean response of the experimental runs, b_i is the estimated coefficient while Ei is the experimental error for the factors, A and B.

Table 1
Variables in Mixture Design. R15, R11, R8, TAT, YKA and unmodified NLCs were represented as 15, 11, 8, 6, 2 and 0 arginines containing peptides, respectively since R15, R11 and R8 have 15, 11 and 8 arginines, respectively. TAT has 6 and YKA has 2 arginines. However, unmodified NLCs were having no arginines. In addition, various skin depths from 0 to 20, 21 to 40, 41 to 80, 81 to 120, 121 to 160 and 161 to 200 were represented as 20, 40, 80, 120, 160 and 200, respectively.

Coded Values	Actual values	
	Number of arginine groups present in peptide	Skin depth (μm)
−1	0 (unmodified NLCs)	20 (0–20)
−0.6	2 (YKA)	40 (21–40)
−0.2	6 (TAT)	80 (41–80)
0.2	8 (R8)	120 (81–120)
0.6	11 (R11)	160 (121–160)
1	15 (R15)	200 (161–200)

Table 2
Presentation of experiments with actual values for factor levels in mixture design with their responses for percent fluorescence and Raman intensity. (ES—Experimental sequesnce). Each experiment was performed using 6 replicates of different nanoparticles and different skin sample at particular depth.

ES*	No of arginine groups in peptide	Skin depth	Percent fluorescence intensity ± SD	Raman intensity ± SD
1	8	40	6.42 ± 0.24	5675.89 ± 389.43
2	11	80	13.21 ± 0.30	12068.46 ± 468.12
3	15	80	6.35 ± 0.32	5015.65 ± 342.51
4	6	40	7.52 ± 0.31	6951.88 ± 314.46
5	2	40	5.24 ± 0.26	4220.13 ± 268.24
6	0	40	4.31 ± 0.24	2825.61 ± 300.42
7	15	200	1.36 ± 0.04	649.10 ± 152.36
8	11	40	15.12 ± 0.45	14041.70 ± 452.34
9	0	120	1.56 ± 0.16	456.23 ± 60.08
10	2	80	3.26 ± 0.22	2291.08 ± 63.16
11	0	160	0.53 ± 0.02	190.26 ± 86.67
12	11	160	9.10 ± 0.15	8066.12 ± 321.34
13	11	200	6.84 ± 0.12	5097.89 ± 316.49
14	11	120	12.96 ± 0.30	11015.35 ± 386.38
15	2	20	6.52 ± 0.26	5220.13 ± 350.89
16	8	80	5.37 ± 0.24	4404.48 ± 322.53
17	6	80	5.53 ± 0.26	5565.16 ± 292.72
18	8	200	0.74 ± 0.08	86.89 ± 6.41
19	2	120	2.06 ± 0.17	456.23 ± 278.94
20	6	200	0.81 ± 0.06	689.23 ± 186.28
21	15	20	10.25 ± 0.40	9575.20 ± 687.43
22	15	160	3.52 ± 0.128	1805.10 ± 292.19
23	2	160	0.57 ± 0.09	914.36 ± 286.24
24	15	120	5.34 ± 0.25	3733.42 ± 363.48
25	2	200	0	224.56 ± 106.61
26	15	40	7.56 ± 0.38	3015.65 ± 276.74
27	0	200	0	1.14 ± 0.06
28	8	120	3.57 ± 0.19	2424.70 ± 322.67
29	6	20	10.07 ± 0.37	9951.88 ± 653.16
30	11	20	17.19 ± 0.51	16093.10 ± 487.23
31	8	20	9.24 ± 0.31	7975.89 ± 524.48
32	6	160	3.18 ± 0.11	2655.90 ± 279.87
33	8	160	2.71 ± 0.10	1497.23 ± 334.67
34	0	20	5.14 ± 0.32	3825.61 ± 316.97
35	6	120	4.23 ± 0.21	3831.90 ± 289.48
36	0	80	2.63 ± 0.20	1823..53 ± 202.43

2.5. Optimization of responses using desirability function

The multiple response method makes use of an objective function called the desirability function. It reflects the desirable ranges for each response (di) [33]. The desirability for each response can be calculated at a given point in the experimental domain. The optimum is the point with the highest value for the desirability.

The percent fluorescence and Raman intensity was targeted to maximum in the procedure, as higher values of this confirm the transport of the fluorescent dye into the deeper skin layers. So the desirability function of this parameter was calculated by using Eq. (2):

$$di = \left(\frac{Yi - Y\min}{Y\max - Y\min}\right)^S \quad (2)$$

where di is individual desirability and Yi is experimental results of percent fluorescence intensity and Raman intensity.

2.6. In vivo confocal laser scanning microscopy (CLSM)

In order to track the fluorescence from surface modified and unmodified NLC the *in vivo* permeation experiments were conducted topically on the skin of Hairless rats (CD® (SD)HrBi, Male). The skin permeation studies were performed under un-occlusive conditions where water evaporation was allowed. CD®(SD) hrBi hairless rats were anaesthetized with an intraperitoneal injection of urethane (1.5 g/kg) and placed on a temperature controlled heating pad (32 ± 1 °C). Six donor chambers were attached on the back of each animals using

cynoacrylate glue (Loctite Super Glue, Avon, OH). 200 μl of nanoparticle dispersion in water (NLC or NLC-R11) was applied into the each donor chambers and carefully spread on the exposed skin area. In all subsequent skin permeation studies similar conditions were maintained. After 24 h, the donor chambers were removed and the exposed skin surface area was then washed with 50% v/v ethanol and blotted dry with lint-free absorbent wipes. Then the animal was sacrificed, the dorsal skin was excised and the adherent fat and subcutaneous tissue were removed. The entire dosing area (0.64 cm^2) was collected with a biopsy punch. To visualize the skin associated fluorescence, skin was fixed on the cryotome stage (Shandon Scientific Ltd, England) using super glue (Loctite Super Glue, Avon, OH) and thin lateral skin sections were collected. The minimum thickness of skin sections to be taken using cryotome is 10 μm. Based on this, initial two sections of 20 μm were collected using cryotome, followed by 40 μm lateral skin sections to represent the total skin depth of 240 μm.

For nuclei staining, the skin sections were incubated with the Hoechst dye solution (1 μg/μl), prepared in PBS (pH 7.4) for 30 min in the dark. The sections were then washed two times with PBS (pH 7.4). Then skin sections were visualized with a laser confocal microscope (Leica Microsystems Inc, Buffalo Grove, IL) using 10× objective. The instrument settings were kept constant for DiO-NLC-CPP and DiO-NLC treated samples. Finally, to improve the results of confocal study, the collected images were analyzed using Digital image software (Museum of Science, Boston, MA) for the skin associated fluorescence.

2.7. In vivo Raman confocal spectroscopy

The lateral rat skin sections of the DID-NLC, DID-NLC-CPP and DID-NLC-YKA were collected as explained for CLSM and observed with HR800 Raman spectroscopy (Horiba Jobin Yvon, NJ) for fluorescence intensity by positioning the skin sections on microscope stage. Raman confocal spectroscopy was calibrated and set as reported by Patlolla et al. [24]. Briefly, 10× objective and 200 mm confocal pin hole were used to acquire the fluorescence data. Throughout the study, all instrument settings were kept constant and exposure time never exceeded 20 sec. For control, the Raman spectrum of untreated rat skin sections was collected as a function of depth upto 240 μm. Raman spectra of DID-NLC-CPP, DID-NLC and DID-NLC-YKA in skin permeation samples were acquired over a 200–1600 cm^{-1} range.

2.8. In vitro skin permeation studies

Hairless rats (CD® (SD)HrBi, Male) were sacrificed by an overdose of halothane anesthesia. The skin from the dorsal surface was excised and the adherent fat and subcutaneous tissue were removed. Rat skin was then immersed in 15% w/v glycerin containing saline solution for 30 min to retain the integrity of the skin and stored at −22 °C for a week based on our earlier work where we have shown that the skin permeation of melatonin and nimesulide was similar to the fresh rat skin even after storing rat skin at −22 °C for 60 days [34]. Prior to the experiments, rat skin was thawed and washed with deionized water. Skin permeation studies were performed under un-occlusive conditions using established procedures by mounting the rat skin on Franz diffusion cell (Permegear Inc., Riegelsville, PA). The surface area of the rat skin exposed to the formulation in the donor chamber was 0.64 cm^2 and the receiver fluid volume was 5 ml. 200 μl of solution, NLC and NLC-R11 formulations containing 0.025% w/w SP and 0.05% w/w KP were applied evenly on the surface of the rat skin in the donor compartment. The skin permeation study was performed using 6 diffusion cells and represented as an average of 6 cells. The receiver compartment was filled with 0.5% w/v volpo 20 in PBS (pH 7.4) and stirred at 300 rpm. The temperature of receiver compartment was maintained at 32 ± 0.5 °C using a circulating water bath to simulate the skin temperature at physiological level. To simulate the clinical conditions, a non-occlusive method was followed. After 24 h of skin permeation, the receiver fluid was collected and centrifuged at 13,500 rpm for 15 min and analyzed for drug content using HPLC. For skin collection, the donor compartment was removed and the excess formulation was removed from the surface of the skin using a cotton swab. The skin was then washed with 50% v/v ethanol and blotted dry with lint-free absorbent wipes. The skin was taken out from the diffusion cell and blotted dry with Kimwipes® and the entire dosing area (0.64 cm^2) was punched out with a biopsy punch.

2.9. Drug extraction from rat skin

To detect the drug retained in rat skin layers, the entire dosing area (0.64 cm^2) was collected with a biopsy punch. SC (0–20 μ), epidermis (21–100 μ) and dermis (rest of the skin) were separated using cryotome (Shandon Scientific Ltd, England). SC, epidermis and dermis were minced and boiled with 250 μl PBS (pH 7.4) separately for 10 min at 60 °C. To these samples 250 μl of acetonitrile was added to solublize the drug. All the samples were then centrifuged at 13,500 rpm for 20 min. The supernatant was collected and analyzed by HPLC for drug content.

2.10. In vitro drug release

In vitro drug release studies of NLC or NLC-R11 (200 μl) containing 0.025% w/w SP and 0.05% w/w KP were performed using Franz diffusion cells. A porous membrane of MWCO 50,000 Da (Sigma-Aldrich Co, MO) was used. The membrane was mounted between the donor and receiver compartments of Franz diffusion cells [35]. The NLC or NLC-R11 dispersion was then applied evenly on the surface of the membrane in the donor compartment. The receiver compartment was filled with 0.5% w/v volpo in PBS (pH 7.4), stirred at 300 rpm and maintained at 32 ± 0.5 °C using circulating water bath. At predetermined time intervals (1, 2, 4, 6, 8, 12, 22 and 24 h), 0.5 ml samples were collected from the receiver compartment and replaced with fresh buffer solution. The samples collected from receiver compartment were analyzed for drug content using HPLC method.

2.11. HPLC analysis

HPLC system (Waters Corp, Milford, MA) along with a Vydac reverse phase C18 (300 Å pore size silica) analytical column (5 μm, 4.6×250 mm) (GraceVydac, Columbia, MD) were used for the analysis of SP. The mobile phases used for SP were 0.1% v/v TFA in water (solvent A) and 0.1% v/v TFA in acetonitrile (solvent B) and they were run at a gradient of 60:40 to 40:60 (solvent A:B, respectively) for 20 min, with a flow rate of 1.2 ml/min. SP content in the samples was determined at 230 nm.

Waters Symmetry C18 analytical column (5 μm, 4.6×250 mm) was used for analysis of KP. The mobile phases used was 0.025% v/v TFA in water (solvent A) and acetonitrile (solvent B) and they were run at a gradient of 70:30 for 5 min, then 10:90 for 8 min followed by 0:100 (solvent A:B, respectively) with a flow rate of 1 ml/min. KP content in the samples was determined at 255 nm.

2.12. In vivo model for allergic contact dermatitis (ACD)

The ACD model was developed as described by Shah et al. [36,37]. Briefly, the C57BL/6 mice were sensitized on day zero by applying 25 μl of 0.5% v/v DNFB in acetone:olive oil (4:1) on the shaved abdomen. Mice were then challenged on day 5 by epicutaneous application of 25 μl of 0.2% v/v DNFB in acetone:olive oil (4:1) on the right ear in order to induce an ACD response. The left ears were treated with vehicle alone (acetone:olive oil 4:1) and served as an internal control. The ACD response was determined by the degree of ear swelling and compared with that of the vehicle treated contra-lateral ear before DNFB challenge. The increase in ear thickness was measured with a

vernier caliper (Fraction + Digital Fractional Caliper, General Tools & Instruments Co., LLC., New York, NY) at 0, 24, 48 and 72 h. Right ears of the mice were treated with topical application of 50 μl of solution, nanoparticle dispersion in water (NLC and NLC-R11) containing 0.025% w/w SP and 0.05% w/w KP, 2 h after antigen challenge and 3 times a day thereafter for 3 days. Topgraf® was used as a positive control. The ear swelling was measured before the application of drug solution and NLC or NLC-R11. This was considered as 0 h ear thickness. Then the drug solution, NLC or NLC-R11 were applied and the ear thickness was measured at 24, 48, and 72 h. The ACD response was determined by taking a difference between 0 h and other time points.

Combination Index (CI) value [38] was used to evaluate the combined effect of SP and KP. The CI was calculated using following equation:

$$\text{Combination Index(CI)} = \frac{\text{Response of Ketoprofen}}{\text{Response of Combination}} + \frac{\text{Response of SpantideII}}{\text{Response of Combination}} \quad (3)$$

The CI values were interpreted as follows: CI > 1.3: antagonism, CI = 1.1–1.3: moderate antagonism, CI = 0.9–1.1: additive effect, CI = 0.8–0.9: slight synergism, if CI = 0.6–0.8: moderate synergism, CI = 0.4–0.6: synergism, CI = 0.2–0.4: strong synergism.

Histological sections of mice ears were observed after hematoxylin and eosin (H&E) staining with an optical microscope (Olympus America, Melville, NY).

2.13. Statistical analysis

The SP and KP content of the skin tissue was expressed as mg per g of the tissue. Differences between the skin permeation and ACD response of SP + KP solution, SP + KP-NLC and SP + KP-NLC-R11 were examined using ANOVA and Tukey multiple comparison test. Means were compared between two groups by Student's *t* test and between three dose groups by one-way variance analysis (ANOVA). Mean differences with $p < 0.05$ were considered to be significant.

3. Results

3.1. Nanoparticle characterization

The mean particle size of NLCs was found to be 140 ± 16 nm, respectively with polydispersity indices (PI) of 0.18 ± 0.03. The mean particle size of NLC-R8, NLC-R11 and NLC-R15 was increased to 150 ± 20 nm after surface modification of NLCs. The zeta potential of NLCs in double distilled water was found to be −17.54 ± 2.64 mV and further decreased to −8.47 ± 3.43 mV after surface modification of NLC with CPPs. Particle size and zeta potential of NLCs and NLC-CPPs were evaluated for a week and found to be stable for a week. The particle size and zeta potential were unaffected by presence of SP and KP. The entrapment efficiency of SP and KP were 87.43 ± 1.86% and 94.64 ± 2.81%, respectively. The entrapment efficiency of SP and KP was unaffected by surface modification.

3.2. Experimental design

The polynomial equations were used to draw conclusions after considering the magnitude of coefficient. The fitted polynomial equations relating the response to the transformed factors are shown in Table 3. The 3D surface plots and contour plots for variables are shown in Fig. 2.

3.3. In vivo confocal laser scanning microscopy (CLSM)

As shown in Fig. 2 and Table 3, the number of arginines containing peptide had a positive coefficient, while the skin depth had negative coefficient. The percent fluorescence intensity, calculated from confocal microscopy images, was found to be in the range between 0 and 18. The intense fluorescence from DiO-NLC-R11 treated skin was detectable upto 240 μm skin depth. Similarly the fluorescence from DiO-NLC-TAT and DiO-NLC-R15 was detected at 200 μm skin depth. The fluorescence from DiO-NLC, DiO-NLC-YKA and DiO-NLC-R8 was disappeared after 120, 160 and 200 μm skin depth, respectively (Fig. 1). The percent intensity of DiO-NLC-R11 was significantly higher than DiO-NLC and DiO-NLC-YKA at various depths.

Table 3
Results of regression analysis.

Terms	Percent fluorescence intensity		Raman intensity (A.U.)	
	EC	Prob > F	EC	Prob > F
Intercept	6.16	NA	5443.87	NA
A	2.82	0.0001	2590.28	0.0002
B	−3.77	<0.0001	−3630.82	<0.0001
A^2	−2.48	0.0220	−2801.76	0.0088
B^2	0.52	0.6310	858.56	0.4197
AB	−0.94	0.2967	−1225.91	0.1645

EC, Estimated coefficient.

3.4. In vivo Raman confocal spectroscopy

According to Fig. 2 and Table 3, the number of arginines of peptide had a positive coefficient, and skin depth had a negative coefficient. The Raman fluorescence intensity was found to be in the range between 0 and 16093 counts. After 24 h, the fluorescence intensities of DID-NLC-R11 were found to be higher than DID-NLC and other polyarginies. At 120 μm skin depth, the Raman intensities were 456 and 11015 counts for DID-NLC and DID-NLC-R11 treated samples, respectively. At 160 μm skin depth, the intensities for DID-NLC-R11 treated samples were reduced to 8066 counts. Further similar to confocal microscopic observations, the Raman intensity from DID-NLC, DID-NLC-YKA and DID-NLC-R8 was disappeared after 120, 160 and 200 μm skin depth, respectively. The Raman intensity from DiD-NLC-TAT and DiD-NLC-R15 was detectable with a weak signal at 200 μm skin depth. However, an intense signal was observed for DID-NLC-R11 treated samples at a skin depth of 240 μm.

3.5. Optimization using desirability function

Any process can only be authenticated when optimum level of its variables (affecting the process) for a product of good quality characteristics is recognized. Desirability function is an excellent tool for identifying the optimum levels of variables [39].

In this study, all the measured responses for independent variables, which are supposed to affect the skin permeation of the NLCs, are taken into consideration. Number of arginines containing peptide and skin depth has to be maximized, in order to pour desired characteristics in the product. The overall desirability response was calculated from the individual desirability of each of the responses using DOE v6.0.5. The optimized number of arginines containing peptide and skin depth was identified with a desirability value of 0.974 (Fig. 3). Table 4 enlists the optimized values for all the dependent variables.

3.6. In vitro drug release

During *in vitro* drug release studies, the SP and KP release from NLC or NLC-R11 was in a controlled manner (Fig. 4). SP-NLC, SP-NLC-R11, SP + KP-NLC and SP + KP-NLC-R11 showed 31% of release of SP while KP-NLC, KP-NLC-R11, SP + KP-NLC and SP + KP-NLC-R11 showed 77% release of KP within 24 h. This difference in the drug release of SP and KP was expected since KP has molecular weight of 254.28 g/mol while SP has molecular weight of 1668.76 g/mol. Thus,

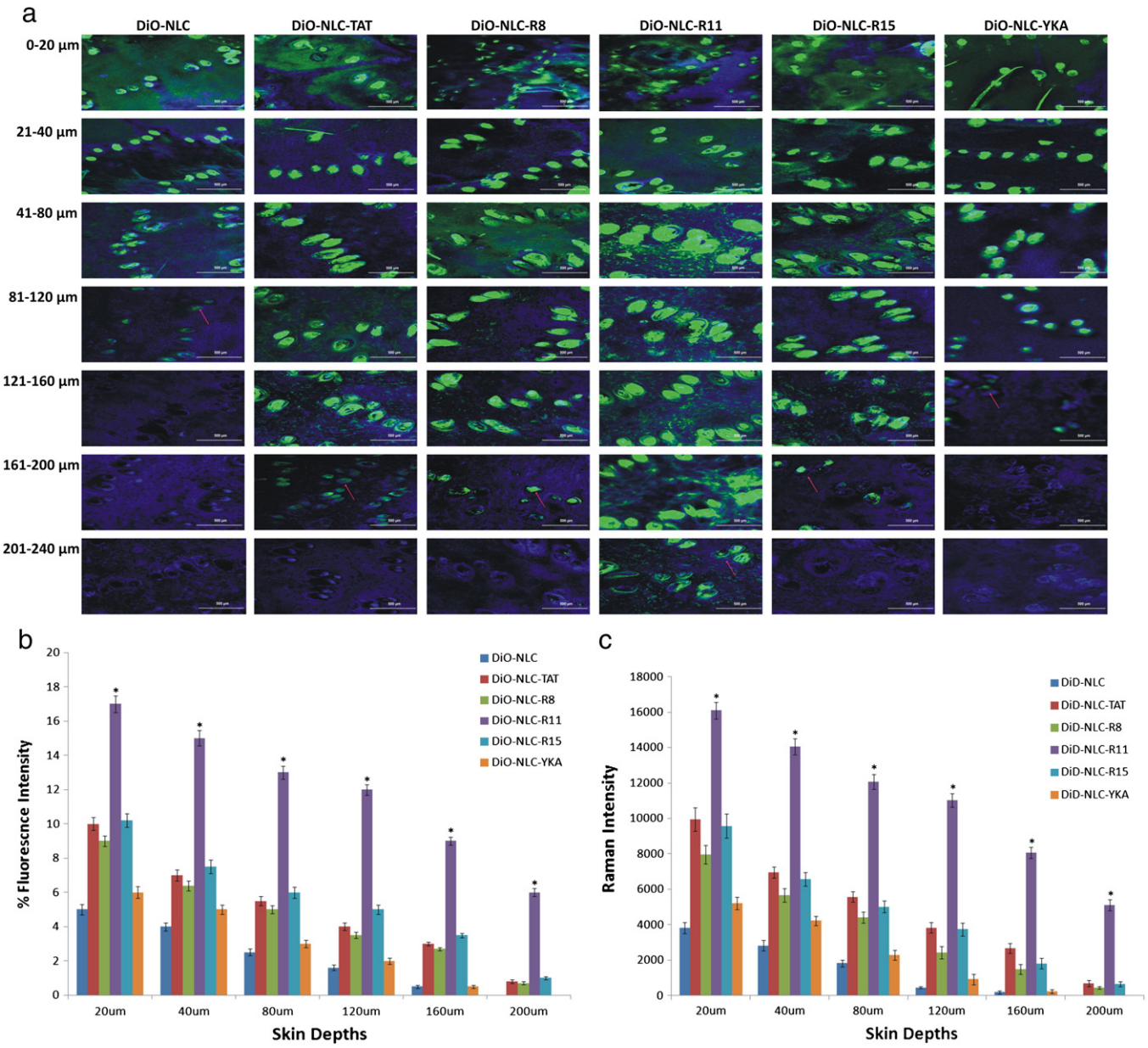

Fig. 1. a) *In vivo* rat skin permeation of fluorescent dye encapsulated, DiO, CPP modified and un-modified NLCs. After 24 h of skin permeation study of CPP modified and unmodified NLCs, the lateral skin sections were cut upto a depth of 240 µm with cryotome and observed with a confocal laser scanning microscope for skin associated fluorescence using 10×. Vertical row indicates the depth of skin sections. The surface modification of NLCs with R11 resulted in increased permeation upto a depth of 240 µm (red arrow). b) Comparison between the percent fluorescence intensity of the DiO encapsulated surface modified and unmodified NLCs for permeated skin sections. Data represent mean ± SD ($n = 6$); significance DiO-NLC-TAT against DiO-NLC-R11, $^{*}p < 0.05$; c) Comparison between the Raman intensity of the DiD encapsulated surface modified and unmodified NLCs for permeated skin sections. Data represent mean ± SD ($n = 6$); significance DiD-NLC-TAT against DiD-NLC-R11, $^{*}p < 0.05$.

KP is expected to be released at faster rate from NLC and NLC-R11 than SP. Drug release from SP-NLC, KP-NLC, SP-NLC-R11, SP + KP-NLC or SP + KP-NLC-R11 was almost similar and followed Korsmeyer–Peppas release kinetics with a best fit r^2 value of 0.99. Further KP-NLC, KP-NLC-R11, SP + KP-NLC or SP + KP-NLC-R11 followed Korsmeyer–Peppas release kinetics with a best fit r^2 value of 0.99. Also there was no significant difference between the drug release from NLC containing only one drug or combination of two drugs.

3.7. In vitro skin permeation

SP and KP levels were detected separately using different analytical columns. Fig. 5 shows the effect of surface modification of NLCs on the skin permeation performed at the end of 24 h. SP was found to be below detectable limits in the receiver compartment for all the formulations. This could be because of the higher molecular weight (1668.76 g/mol) and high lipophilicity (Log P—6.6) of SP. However, NLC-R11 showed significant increase in the SP retention in different skin layers compared to SP-Solution and SP-NLC. The SC, epidermal and dermal retention of SP for SP-NLC-R11 was 10.92, 7.02 and 0.82 mg/g of skin, respectively. The skin retention of SP in various skin layers for SP-NLC-R11 was approximately 2.3 and 1.8 times higher than SP-Solution and SP-NLC, respectively.

In contrast to SP, KP was detected in receiver compartment and 53.35 µg/cm^2 of KP was found to be permeated through rat skin after 24 h for KP-NLC-R11. Further the SC, epidermal and dermal retention of KP for KP-NLC-R11 was 0.75, 0.44 and 0.17 mg/g of skin, respectively. The retention of KP in various skin layers for KP-NLC-R11

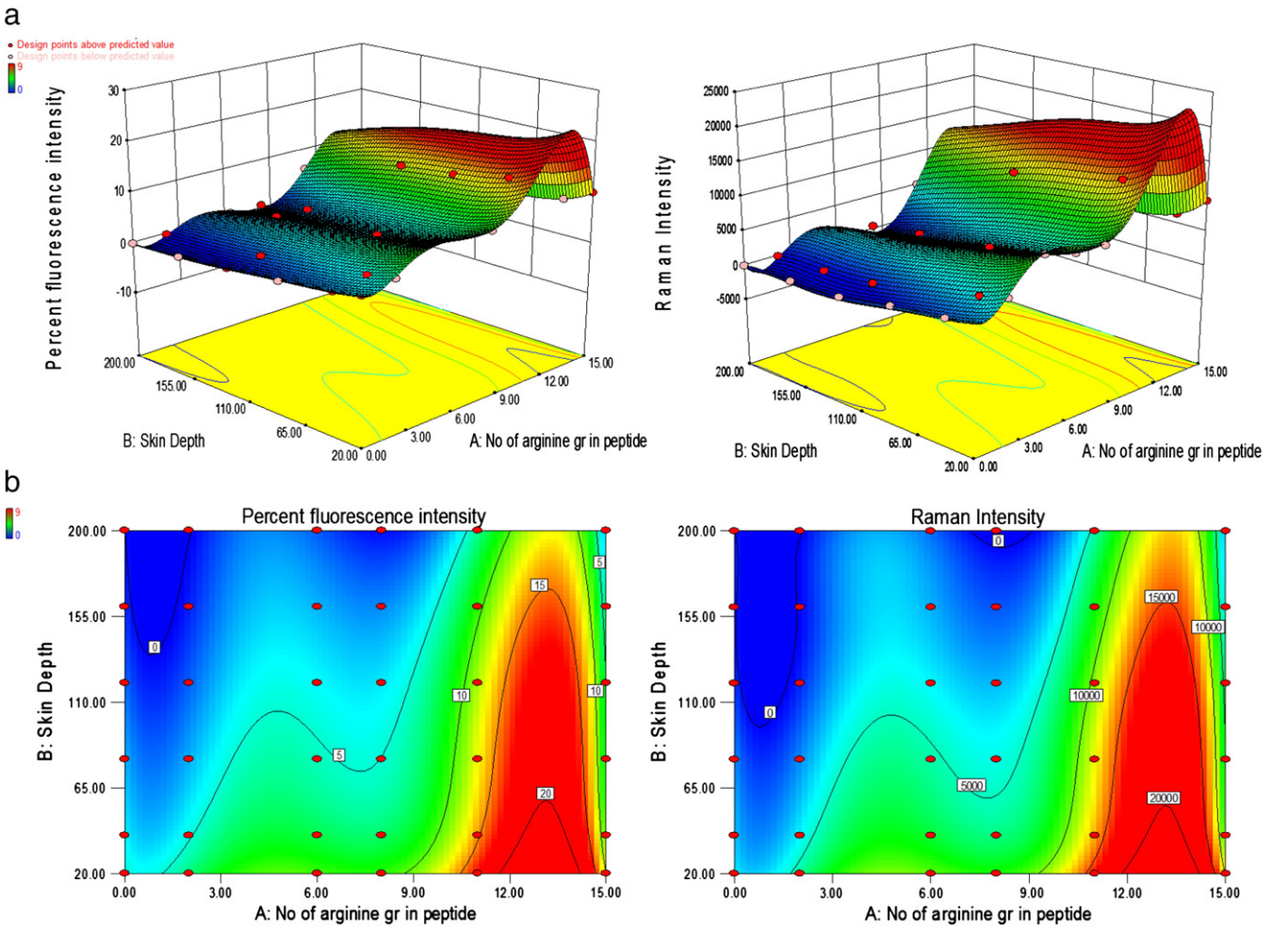

Fig. 2. a) 3D surface plots showing the effect of number of arginines present in peptide and skin depth on the percent fluorescence and Raman intensity of DiO-NLC and DiO-NLC-CPP permeated skin sections.

was approximately 2.8 and 1.6 times higher than KP-Solution and KP-NLC, respectively. The permeated amount of KP was approximately 7.9 and 2.6 times higher than KP-Solution and KP-NLC, respectively. The skin retention of KP was significantly less than the SP. This could be because of the lower molecular weight (254.28 g/mol) and Log P value of 3.1 for KP, assisting in transport of KP across the skin which increases the amount of KP in receiver compartment. The skin retention of SP and KP for SP-NLC-R11 and KP-NLC-R11 was almost similar to SP + KP-NLC-R11 for both the drugs. This indicates that loading of combination of drugs in NLC did not affect the skin permeation characteristics of the individual drugs.

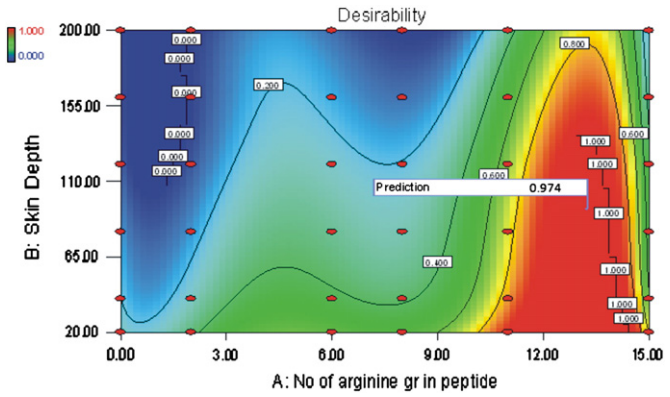

Fig. 3. Response surface plot of desirability function.

3.8. In vivo model for allergic contact dermatitis (ACD)

The reduction of ear swelling in mice was used to monitor the treatment of inflammation after application of various formulations. The effect of KP —, SP — and SP + KP-Solution, KP-NLC, SP-NLC, SP + KP-NLC, KP-NLC-R11, SP-NLC-R11 and SP + KP-NLC-R11 on the reduction of ear swelling is shown in Fig. 6. The ear thickness was increased from 139.46 to 166.79 μm with time for control animals. However, at 72 h, the ear thickness was decreased to 116.24, 108.13 and 84.56 μm for KP-Solution, KP-NLC and KP-NLC-R11, respectively. Similarly, it was 127.43, 113.78 and 88.65 μm for SP-Solution, SP-NLC and SP-NLC-R11, respectively. There was no statistical difference in ear thickness before and after application of Topgraf®. The ear thickness for SP + KP-Solution, SP + KP-NLC and SP + KP-NLC-R11 was found to be 83.43, 60.84 and 31.51 μm, respectively. In addition, the combination index value calculated using ACD model for SP + KP-Solution was 0.98 which suggests additive effect, while for SP + KP-NLC-R11 it was 0.83 indicating slight synergism. The response of ACD model was further characterized by histological examination and the results are presented in Fig. 7. The combination of SP + KP-NLC-R11 was more effective in the treatment of ACD by reducing the ear swelling, compared to control, SP + KP-NLC and SP + KP solution.

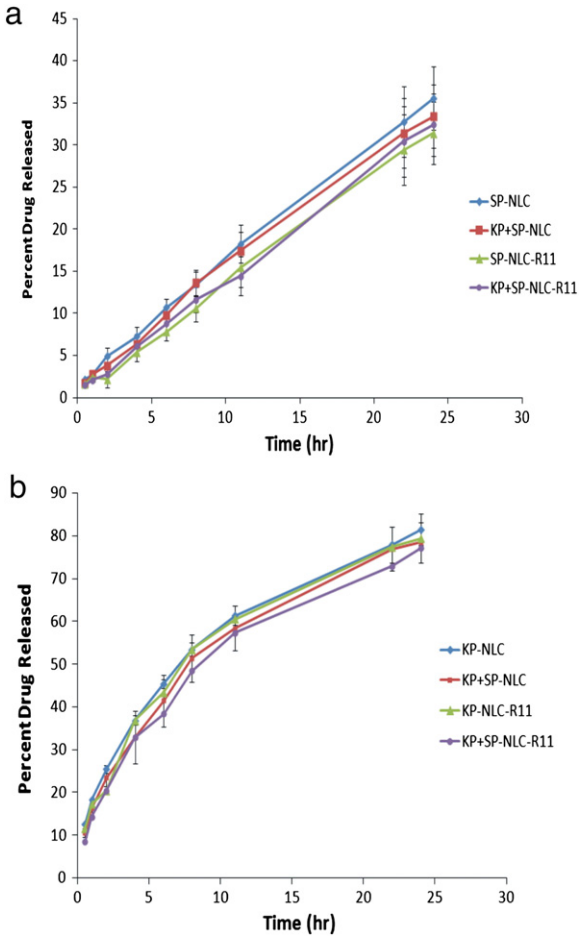

Fig. 4. *In vitro* drug release of i) SP and ii) KP from NLCs or NLC-R11 in PBS (pH 7.4) containing 0.5% w/v volpo 20. The cumulative amount released was plotted against time. The drug release studies with SP-NLC or KP-NLC and SP + KP-NLC showed no significant difference between the KP and SP release when used alone or in combination, signifying no interaction between the drug release of SP and KP. Data represent mean ± SD, $n = 6$.

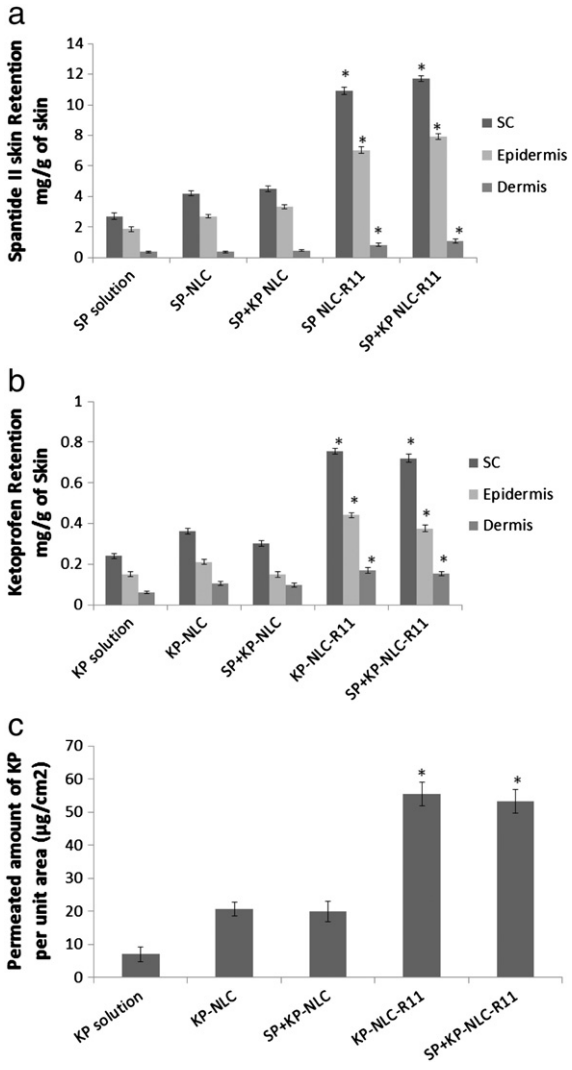

Fig. 5. Effect of control solution, NLC and NLC-R11 on the skin retention of a) SP and b) KP. *In vitro* skin permeation studies were performed in rat skin using Franz diffusion cells and after 24 h of application, the skin was collected and processed as described in Materials and methods. The amount of SP and KP retained in SC, epidermis and dermis after application of NLC-R11 is significantly higher than control solution and NLC. c) The amount of KP permeated per unit area after 24 hrs of rat skin permeation study, performed using control solution, NLC and NLC-R11. Data represent mean ± SD, $n = 6$, significance control solution against NLC-R11 where $^*p < 0.05$.

4. Discussion

ACD is the most common inflammatory skin disorder and for its topical treatment, it is desirable to deliver the drug into the deeper skin layers. Lipid based nanoparticles (SLN and NLCs) show excellent adhesion, skin hydration and occlusion effects when applied topically on skin. These properties are mainly dependent on their size since smaller particles show higher barrier properties for evaporation of water due to increase in surface area [40]. It is also believed that rigid particles above 10 nm do not penetrate the intact skin [41]. Therefore to enhance the transport of drugs across the skin layers, there is a need for the surface modification of lipid based nanoparticles. Our laboratory has demonstrated that the surface modification of NLCs with TAT, a well known CPP having 6 arginines, can effectively enhance the skin permeation of fluorescent dye (DIO) and celecoxib [24]. These results are in agreement with other studies, where TAT and AT1002 analogs were used in combination to deliver

Table 4
Individual and overall desirability of measured responses.

Resposes	Desirability
Percent fluorescence intensity	0.965
Raman intensity	0.974
Overall desirability	0.974

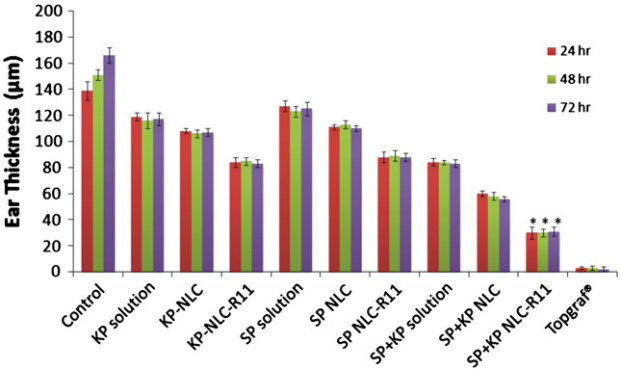

Fig. 6. Effect of control solution, NLC and NLC-R11 containing SP and KP treatment on the response of ACD model in C57BL/6 mice. Data represent mean ± SD, $n = 6$; significance solution against NLC-R11, $^*p < 0.05$.

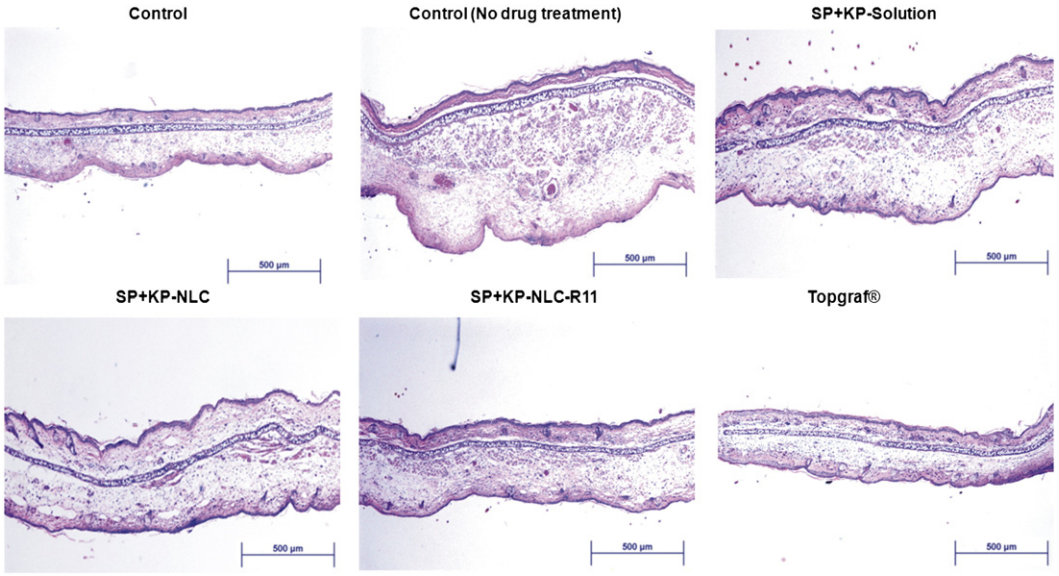

Fig. 7. H&E staining of inflammation induced by topical application of DNFB, and after 72 h treatment of SP + KP solution SP + KP-NLC and a positive control, Topgraf®. The images were captured using 10× magnifications.

siRNA across mice skin and were reported to have permeation-enhancing ability across the skin [42].

Various mechanisms like diffusion through intercellular lipids, corneocytes and/or appendages have been suggested for permeation enhancing ability of CPPs. Work conducted in our laboratory has hypothesized the following sequence of events after application of NLC-CPP on the skin, firstly the positively charged CPPs interacts with the negatively charged residues of proteins and lipids of SC. Once the peptide aggregation reaches a critical size, a transitional destabilization of the membrane occurs which allows enhanced permeation of NLCs and its payloads [24]. Similar results were proposed for penetratin (RQIKIWFQNRRMKWKK), a well known CPP, which is reported to destabilize SC lipid bilayers in the intercellular regions leading to an overall increase in membrane permeability of the NLC and encapsulated drug molecules [19,43]. Another penetration enhancing pathway for CPPs is through interaction with corneocyte protein, keratin. Recent studies with SPACE peptide (AC-TGSTQHQ-CG) showed a potential to enhance the partitioning into SC by impacting keratin structure without disturbing SC lipids [44]. Lastly the penetration pathway is through appendages [45] where CPP conjugated nanoparticles penetrates and accumulates into hair follicles and sebaceous glands which acts as a reservoir. Further, based on the physicochemical properties, the drug released from nanoparticles diffuses into the skin layers or receiver compartment. Collectively, NLC-CPP can follow more than one penetration pathway to enhance permeation of intact NLCs and encapsulated drug. Although a variety of mechanisms for the permeation enhancing ability of CPPs have been suggested, parameters such as charge, primary sequence, length and linearity of peptides can influence the translocation efficiency of CPPs.

Among several CPPs, TAT is known to have higher permeation enhancing ability which is mainly because of the presence of cationic amino acids like arginines and lysines. TAT is comprised of 6 arginines and 2 lysines. Polyarginine peptide containing more than 6 arginine groups might result in enhanced permeation and thus improved skin permeation. Also polyarginines are known to have significantly higher permeation enhancing ability than TAT and other cationic polypeptides in terms of cell internalization [46]. Similar results were reported for polyarginine containing peptides where a polyarginine peptide containing 9 arginines (RRRRRRRRR; NONA) showed significant increase in skin permeation of sodium diclofenac containing reversed hexagonal liquid crystals ($H_{II}LC$) compared to control $H_{II}LC$ and other peptides like RALA (RALARALARALRALAR) [27,28]. This could be because of presence of 9 arginines in peptide. Further in this study, NONA was present inside $H_{II}LC$ and not on the surface of $H_{II}LC$ which might result in comparatively less skin permeation because of the delayed contact time between the skin and NONA peptide. Therefore it is important to have polyarginine peptides on the surface of nanoparticles to reduce the contact time between polyarginines and skin which would result in maximum skin permeation. No study has been reported on the use of polypeptide with different chain length of arginines.

This is the first study to investigate the effect of polyarginine chain length for delivery of NLCs across the skin and correlate *in vitro* data with *in vivo* experiments. Further design of experiments (DOE) was used to investigate the permeation enhancing ability of polyarginine peptide modified NLCs into the skin. Various statistical designs like Box-Behnken [47], central composite [48], Taguchi and factorial design [49,50] are available. However, they can be used only at 3 levels. In the present study, we have used 2 independent variables (number of arginines containing peptide and skin depths) which were evaluated at 6 different levels. Therefore a user defined mixture design was chosen for optimization of polyarginines for surface modification of NLCs to improve skin permeation.

The confocal microscopic studies demonstrated that the distribution of fluorescence from DiO-NLC was limited to the surface of the skin and to the hair follicles, because of the higher particle size (150 nm) which restricts the NLCs to penetrate through the SC [1]. However, DiO-NLC-CPP showed significant distribution of fluorescence into the epidermis and dermis. This is mainly because of the significant permeation-enhancing ability of the CPPs through a variety of mechanisms, including disruption of the barrier layer of the skin and the CPP's ability to carry NLC containing fluorescent dye into the skin as it penetrates [19]. Preliminary investigations of the process parameters revealed that the percent fluorescence and Raman intensity were highly influenced by the factors like number of arginines containing peptide (A) and skin depth (B). Therefore, a number of arginines containing peptide (A) and skin depth (B) were used as independent variables while percent fluorescence and Raman intensity were selected as dependent variables. Based on analysis of variance (ANOVA), higher correlation coefficient (r^2) values for dependent variables indicated a good model fit (Table 4). Similar results were reported for preparation of mefloquine hydrochloride encapsulated chitosan microparticles where the amount of drug, polymer and crosslinking agent were used as independent variables while bitterness, incorporation efficiency, particle size,

and drug release were used as dependent variables [32]. The correlation coefficient (r^2) values for all dependent variables ranged from 0.96 to 0.98, signifying a good model fit. According to the 3D surface plot and contour plot, polyarginine peptide containing 11 arginines showed significant effect on percent fluorescence and Raman intensity than other polyarginines containing different arginines chain length (Fig. 2). Further the desirability calculated from the experimental design showed a prediction value of 0.974, signifying that polyarginine chain length of 11 arginines (R11) was the optimal length of peptide to show CPP oriented permeation enhancing ability into the skin. In addition, the percent fluorescence and Raman intensity of NLC-R11 was significantly higher ($p<0.05$) than NLC-TAT (Fig. 1b and c). This might be because of the optimum positive charge of the polyarginine (R11) required in transporting NLCs encapsulated drugs across the skin depths since TAT has only 6 arginines. However, the response for NLC-R15 in terms of percent fluorescence and Raman intensity was significantly less than NLC-R11 possibly due to super saturation effect or because of the hindrance effect from longer chain length. The results of confocal microscopy and Raman confocal spectroscopy for TAT and YKA modified NLCs are in agreement with our earlier reported *in vitro* confocal microscopy and Raman confocal spectroscopy observations of TAT and YKA modified NLCs [24]. Thus, based on the results of desirability, R11 peptide was selected for preparation of SP and KP containing NLCs. These NLCs and NLC-R11 were further evaluated for *in vitro* drug release and skin permeation studies along with *in vivo* therapeutic response using ACD model.

For confocal microscopy and Raman confocal spectroscopy studies, we used compritol (melts above 60 °C) as a solid lipid to prepare NLCs. However SP is a synthetic peptide and is less stable at high temperature (above 60 °C) [51]. Compritol when mixed with precirol, showed slight reduction in the melting temperature of compritol [52]. Similarly monosterol and precirol were mixed together in the present study to reduce the melting temperature of precirol to 45–50 °C where SP is stable [51]. In addition, to stabilize SP in NLC, L-phospatidylinositol (PI) was added in a lipid phase to protect the α-helical secondary structure of SP which was confirmed by circular dichroism spectroscopy (unpublished data). *In vitro* drug release from SP-NLC and KP-NLC followed Korsmeyer–Peppas kinetics suggesting that the SP and KP were released in a controlled manner by a combination of both diffusion and erosion mechanisms. Further the *in vitro* drug release from NLC and NLC-R11 was not significantly different since there was no barrier layer similar to SC.

During skin permeation studies, NLCs modified with R11 peptide showed significant increase in the skin permeation of SP and KP in various skin layers compared to control SP + KP-Solution and SP + KP-NLC (Fig. 4). Similar results were observed for oleic acid modified PLGA-chitosan bilayered nanoparticles and its nanogel (Nano-ease technology) comprising SP and KP [36,37]. The skin permeation of SP and KP nanogel was significantly higher than PLGA-chitosan bilayered nanoparticles and SP + KP solution after 24 h of dermatomed human skin permeation study, signifying that the surface modification of nanoparticles is required to deliver the active drug to the deeper skin layers.

Further during inflammation SP blocks the inflammatory effects of substance P by competitively binding to neurokinin-1 receptors on cutaneous cells [2–4] and KP inhibits prostaglandin biosynthesis along with the maturation of Langerhans cells [6]. Therefore, the effect of SP and KP containing NLC and NLC-R11 on inflammatory response was further investigated using ACD model. The ear thickness after topical application of SP + KP-NLC-R11 was significantly less ($p<0.05$) than SP + KP-Solution and SP + KP-NLC (Fig. 6). Further, topical treatment of SP + KP-NLC-R11 resulted in a reduction of both cutaneous edema and the number of leukocytes infiltrating into the skin compared to the ACD response of untreated control mice as shown in Fig. 7. However Topgraf®, a commercial tacrolimus formulation was more effective ($p<0.05$) than the SP + KP-NLC-R11 which was expected since tacrolimus is a non-steroidal immunosuppressant and has shown notable efficacy in ACD [53–55]. The combination index value suggested slight synergism for NLC-R11 over the entire study period. This observation supports the hypothesis that the reduction of ear thickness for NLC-R11 was mainly because of the enhanced delivery of both the drugs by surface modification of NLC with R11 and impact of two different mechanisms working in cohort to minimize inflammation associated with ACD.

5. Conclusion

Our studies demonstrate that response surface methodology could be used to optimize the peptide modification on nanoparticles required to enhance skin permeation of drugs. Fluorescent dye encapsulated NLCs modified with R11 peptide showed distinct fluorescence at 240 μm skin depth compared to other peptides. Surface modified NLCs showed enhanced skin permeation of spantide II and ketoprofen to the deeper skin layers which were further responsible for improved response in reducing the ear thickness and inflammation associated with ACD. This suggests the potential of the combination therapy to treat inflammatory skin disease like ACD. These results could be further applicable to various other skin disorders like psoriasis, fungal, bacterial, viral infections and skin cancers like melanoma.

Acknowledgements

We thank Dr. Geoffrey Strouse, Department of Biomedical Sciences, Florida State University, Tallahassee, FL for providing confocal microscopy facility and Dr. Kalayu Belay, Department of Physics Florida A&M University, Tallahassee, FL for their kind help in Raman confocal spectroscopy studies. We thank Dr Ram Patlolla for his technical inputs. This project was supported by the National Center for Research Resources and the National Institute of Minority Health and Health Disparities of the National Institutes of Health through grant numbers8G12 MD007582-28 and 2G12 RR003020.

References

[1] L.B. Jensen, K. Petersson, H.M. Nielsen, In vitro penetration properties of solid lipid nanoparticles in intact and barrier-impaired skin, Eur. J. Pharm. Biopharm. 79 (2011) 68–75.
[2] H. Inoue, N. Nagata, Y. Koshihara, Involvement of substance P as a mediator in capsaicin-induced mouse ear oedema, Inflamm. Res. 44 (1995) 470–474.
[3] R.J. Babu, L. Kikwai, L. Jaiani, N. Kanikkannan, C. Armstrong, J. Ansel, M. Singh, Percutaneous absorption and anti-inflammatory effect of a substance P receptor antagonist: spantide II, Pharm. Res. 21 (2004) 108–113.
[4] L. Kikwai, R.J. Babu, R. Prado, A. Kolot, C.A. Armstrong, J.C. Ansel, M. Singh, In vitro and in vivo evaluation of topical formulations of spantide II, AAPS PharmSciTech 6 (2005) E565–E572.
[5] N. Shinkai, K. Korenaga, Y. Okumura, H. Mizu, H. Yamauchi, Microdialysis assessment of percutaneous penetration of ketoprofen after transdermal administration to hairless rats and domestic pigs, Eur. J. Pharm. Biopharm. 78 (2011) 415–421.
[6] K. Atarashi, K. Kabashima, K. Akiyama, Y. Tokura, Skin application of the nonsteroidal anti-inflammatory drug ketoprofen downmodulates the antigen-presenting ability of Langerhans cells in mice, Br. J. Dermatol. 159 (2008) 306–313.
[7] L. Kikwai, R.J. Babu, N. Kanikkannan, M. Singh, Preformulation stability of Spantide II, a promising topical anti-inflammatory agent for the treatment of psoriasis and contact dermatitis, J. Pharm. Pharmacol. 56 (2004) 19–25.
[8] M.M. Abdel-Mottaleb, D. Neumann, A. Lamprecht, Lipid nanocapsules for dermal application: a comparative study of lipid-based versus polymer-based nanocarriers, Eur. J. Pharm. Biopharm. 79 (2011) 36–42.
[9] P. Karande, A. Jain, S. Mitragotri, Insights into synergistic interactions in binary mixtures of chemical permeation enhancers for transdermal drug delivery, J. Control. Release 115 (2006) 85–93.
[10] B. Barry, Mode of action of penetration enhancers in human skin, J. Control. Release 6 (1987) 85–97.
[11] B. Polat, D. Hart, R. Langer, D. Blankschtein, Ultrasound-mediated transdermal drug delivery: mechanisms, scope, and emerging trends, J. Control. Release 152 (2011) 330–348.
[12] A. Sintov, I. Krymberk, D. Daniel, T. Hannan, Z. Sohn, G. Levin, Radiofrequency-driven skin microchanneling as a new way for electrically assisted transdermal delivery of hydrophilic drugs, J. Control. Release 89 (2003) 311–320.
[13] Y. Henchoz, N. Abla, J. Veuthey, P. Carrupt, A fast screening strategy for characterizing peptide delivery by transdermal iontophoresis, J. Control. Release 137 (2009) 123–129.

[14] H. Chen, H. Zhu, J. Zheng, D. Mou, J. Wan, J. Zhang, T. Shi, Y. Zhao, H. Xu, X. Yang, Iontophoresis-driven penetration of nanovesicles through microneedle-induced skin microchannels for enhancing transdermal delivery of insulin, J. Control. Release 139 (2009) 63–72.

[15] S. Murthy, S. Sammeta, C. Bowers, Magnetophoresis for enhancing transdermal drug delivery: mechanistic studies and patch design, J. Control. Release 148 (2010) 197–203.

[16] R. Vanbever, G. Langers, S. Montmayeur, V. Préat, Transdermal delivery of fentanyl: rapid onset of analgesia using skin electroporation, J. Control. Release 50 (1998) 225–235.

[17] S. Bal, A. Kruithof, R. Zwier, E. Dietz, J. Bouwstra, J. Lademann, M. Meinke, Influence of microneedle shape on the transport of a fluorescent dye into human skin in vivo, J. Control. Release 147 (2010) 218–224.

[18] G. Cevc, U. Vierl, Nanotechnology and the transdermal route: a state of the art review and critical appraisal, J. Control. Release 141 (2010) 277–299.

[19] P. Desai, R.R. Patlolla, M. Singh, Interaction of nanoparticles and cell-penetrating peptides with skin for transdermal drug delivery, Mol. Membr. Biol. 27 (2010) 247–259.

[20] K. Mitri, R. Shegokar, S. Gohla, C. Anselmi, R.H. Muller, Lipid nanocarriers for dermal delivery of lutein: preparation, characterization, stability and performance, Int. J. Pharm. 414 (2011) 267–275.

[21] M. Schafer-Korting, W. Mehnert, H.C. Korting, Lipid nanoparticles for improved topical application of drugs for skin diseases, Adv. Drug Deliv. Rev. 59 (2007) 427–443.

[22] P.V. Pople, K.K. Singh, Targeting tacrolimus to deeper layers of skin with improved safety for treatment of atopic dermatitis, Int. J. Pharm. 398 (2010) 165–178.

[23] V. Teeranachaideekul, P. Boonme, E. Souto, R. Müller, V. Junyaprasert, Influence of oil content on physicochemical properties and skin distribution of nile red-loaded NLC, J. Control. Release 128 (2008) 134–141.

[24] R.R. Patlolla, P.R. Desai, K. Belay, M.S. Singh, Translocation of cell penetrating peptide engrafted nanoparticles across skin layers, Biomaterials 31 (2010) 5598–5607.

[25] S.B. Fonseca, M.P. Pereira, S.O. Kelley, Recent advances in the use of cell-penetrating peptides for medical and biological applications, Adv. Drug Deliv. Rev. 61 (2009) 953–964.

[26] K. Kigasawa, K. Kajimoto, T. Nakamura, S. Hama, K. Kanamura, H. Harashima, K. Kogure, Noninvasive and efficient transdermal delivery of CpG-oligodeoxynucleotide for cancer immunotherapy, J. Control. Release 150 (2011) 256–265.

[27] M. Cohen-Avrahami, A. Aserin, N. Garti, H(II) mesophase and peptide cell-penetrating enhancers for improved transdermal delivery of sodium diclofenac, Colloids Surf. B Biointerfaces 77 (2010) 131–138.

[28] M. Cohen-Avrahami, D. Libster, A. Aserin, N. Garti, Sodium diclofenac and cell-penetrating peptides embedded in H(II) mesophases: physical characterization and delivery, J. Phys. Chem. B 115 (2011) 10189–10197.

[29] S. Futaki, Membrane-permeable arginine-rich peptides and the translocation mechanisms, Adv. Drug Deliv. Rev. 57 (2005) 547–558.

[30] A. Jones, E. Sayers, Cell entry of cell penetrating peptides: tales of tails wagging dogs, J. Control. Release 161 (2012) 582–591.

[31] N. Mennini, S. Furlanetto, M. Cirri, P. Mura, Quality by design approach for developing chitosan-Ca-alginate microspheres for colon delivery of celecoxib-hydroxypropyl-β-cyclodextrin–PVP complex, Eur. J. Pharm. Biopharm. 80 (2012) 67–75.

[32] P.P. Shah, R.C. Mashru, Influence of chitosan crosslinking on bitterness of mefloquine hydrochloride microparticles using central composite design, J. Pharm. Sci. 98 (2009) 690–703.

[33] P.P. Shah, R.C. Mashru, Y.M. Rane, A.C. Badhan, Design and optimization of artemether microparticles for bitter taste masking, Acta Pharm. 58 (2008) 379–392.

[34] R. Babu, N. Kanikkannan, L. Kikwai, C. Ortega, S. Andega, K. Ball, S. Yim, M. Singh, The influence of various methods of cold storage of skin on the permeation of melatonin and nimesulide, J. Control. Release 86 (2003) 49–57.

[35] N. Ghouchi Eskandar, S. Simovic, C.A. Prestidge, Nanoparticle coated submicron emulsions: sustained in-vitro release and improved dermal delivery of all-trans-retinol, Pharm. Res. 26 (2009) 1764–1775.

[36] P.P. Shah, P.R. Desai, A. Patel, M. Singh, Skin permeating nanogel for the cutaneous co-delivery of two anti-inflammatory drugs, Biomaterials 33 (2012) 1607–1617.

[37] P.P. Shah, P.R. Desai, M. Singh, Effect of oleic acid modified polymeric bilayered nanoparticles on percutaneous delivery of spantide II and ketoprofen, J. Control. Release 158 (2011) 336–345.

[38] M. Chougule, A.R. Patel, P. Sachdeva, T. Jackson, M. Singh, Anticancer activity of noscapine, an opioid alkaloid in combination with cisplatin in human non-small cell lung cancer, Lung Cancer 71 (2012) 271–282.

[39] A.C. Badhan, R.C. Mashru, P.P. Shah, A.R. Thakkar, N.B. Dobaria, Development and evaluation of sustained release gastroretentive minimatrices for effective treatment of H. pylori infection, AAPS PharmSciTech 10 (2009) 459–467.

[40] E.B. Souto, R. Müller, Cosmetic features and applications of lipid nanoparticles (SLN, NLC), Int. J. Cosmet. Sci. 30 (2008) 157–165.

[41] W.C. Mak, H. Richter, A. Patzelt, W. Sterry, K.K. Lai, R. Renneberg, J. Ladermann, Drug delivery into the skin by degradable particles, Eur. J. Pharm. Biopharm. 79 (2011) 23–27.

[42] T. Uchida, T. Kanazawa, Y. Takashima, H. Okada, Development of an efficient transdermal delivery system of small interfering RNA using functional peptides, Tat and AT-1002, Chem. Pharm. Bull.(Tokyo) 59 (2011) 196–201.

[43] M. Cohen-Avrahami, D. Libster, A. Aserin, N. Garti, Penetratin-induced transdermal delivery from H(II) mesophases of sodium diclofenac, J. Control. Release 159 (2012) 419–428.

[44] T. Hsu, S. Mitragotri, Delivery of siRNA and other macromolecules into skin and cells using a peptide enhancer, Proc. Natl. Acad. Sci. U.S.A. 108 (2011) 15816–15821.

[45] F. Knorr, J. Lademann, A. Patzelt, W. Sterry, U. Blume-Peytavi, A. Vogt, Follicular transport route—research progress and future perspectives, Eur. J. Pharm. Biopharm. 71 (2009) 173–180.

[46] D.J. Mitchell, D.T. Kim, L. Steinman, C.G. Fathman, J.B. Rothbard, Polyarginine enters cells more efficiently than other polycationic homopolymers, J. Pept. Res. 56 (2000) 318–325.

[47] P. Dayal, V. Pillay, R.J. Babu, M. Singh, Box-Behnken experimental design in the development of a nasal drug delivery system of model drug hydroxyurea: characterization of viscosity, in vitro drug release, droplet size, and dynamic surface tension, AAPS PharmSciTech 6 (2005) E573–E585.

[48] P.P. Shah, R.C. Mashru, A.R. Thakkar, A.C. Badhan, Effect of chitosan crosslinking on bitterness of artemether using response surface methodology, J. Pharm. Pharmacol. 60 (2008) 421–427.

[49] Y.M. Rane, R.C. Mashru, M.G. Sankalia, V.B. Sutariya, P.P. Shah, Investigations on factors affecting chitosan for dissolution enhancement of oxcarbazepine by spray dried microcrystal formulation with an experimental design approach, Drug Dev. Ind. Pharm. 33 (2007) 1008–1023.

[50] P.P. Shah, R.C. Mashru, Y.M. Rane, A. Thakkar, Design and optimization of mefloquine hydrochloride microparticles for bitter taste masking, AAPS PharmSciTech 9 (2008) 377–389.

[51] L. Kikwai, R.J. Babu, N. Kanikkannan, M. Singh, Stability and degradation profiles of spantide II in aqueous solutions, Eur. J. Pharm. Sci. 27 (2006) 158–166.

[52] J. Hamdani, A.J. Moës, K. Amighi, Physical and thermal characterisation of precirol and compritol as lipophilic glycerides used for the preparation of controlled-release matrix pellets, Int. J. Pharm. 260 (2003) 47–57.

[53] H. Yamashita, T. Ito, H. Kato, S. Asai, H. Tanaka, H. Nagai, N. Inagaki, Comparison of the efficacy of tacrolimus and cyclosporine A in a murine model of dinitrofluorobenzene-induced atopic dermatitis, Eur. J. Pharmacol. 645 (2010) 171–176.

[54] Y.V. Saripalli, J.E. Gadzia, D. Belsito, Tacrolimus ointment 0.1% in the treatment of nickel-induced allergic contact dermatitis, J. Am. Acad. Dermatol. 49 (2003) 477–482.

[55] D. Belsito, D.C. Wilson, E. Warshaw, J. Fowler, A. Ehrlich, B. Anderson, B.E. Strober, J. Willetts, E.S. Rutledge, A prospective randomized clinical trial of 0.1% tacrolimus ointment in a model of chronic allergic contact dermatitis, J. Am. Acad. Dermatol. 55 (2006) 40–46.